Available online at www.sciencedirect.com
ScienceDirect
Electrochimica Acta 52 (2006) 1417–1425
ELECTROCHIMICA Acta
www.elsevier.com/locate/electacta

Optimization of cathode catalyst layer for direct methanol fuel cells Part I. Experimental investigation

Fuqiang Liu, Chao-Yang Wang *

Electrochemical Engine Center (ECEC), and Department of Materials Science and Engineering, The Pennsylvania State University, University Park, PA 16802, United States

Received 19 March 2006; received in revised form 10 July 2006; accepted 3 August 2006
Available online 8 September 2006

Abstract

The cathode catalyst layer (CL) in direct methanol fuel cells (DMFCs) has been optimized through a balance of ionomer and porosity distributions, both playing important roles in affecting proton conduction and oxygen transport through a thick CL of DMFC. The effects of fabrication procedure, ionomer content, and Pt distribution on the microstructure and performance of a cathode CL under low air flowrate are investigated. Electrochemical methods, including electrochemical impedance, cyclic votammetry and polarization curves, are used in conjunction with surface morphology characterization to correlate electrochemical characteristics with CL microstructure. CLs in the form of catalyst-coated membrane (CCM) have higher cell open circuit voltages (OCVs) and higher limiting current density; while catalyzed-diffusion-media (CDM) CLs display better performance in the moderate current density region. The CL with a composite structure, consisting both CCM and CDM, shows better performance in both kinetic and mass-transport limitation region, due to a suitable ionomer distribution across the CL. This composite cathode is further evaluated in a full DMFC and the cathode performance loss due to methanol crossover is discussed.

Keywords: Direct methanol fuel cell; Catalyst layer; Microstructure; Cathode

1. Introduction

An effective cathode catalyst layer (CL) must serve multiple functions simultaneously: electron and proton conduction, oxygen supply and product water removal. Nafion ionomer in the CL provides protonic conduction, and helps to maintain structural integrity and robustness. An optimized cathode CL structure has a good balance between electrochemical activity and oxygen transport capability with effective water removal. There are many experimental studies on the optimization of CL compositions in H_2/air fuel cells. Most of these efforts were focused on optimization of cell performance as a function of Nafion content. Lee et al. [1] evaluated the effect of Nafion loading on charge-transfer resistance and mass transport. Uchida et al. [2,3] investigated the gas-supplying network formed by Nafion colloids. The optimum Nafion weight fraction was reported to be in the range of 30–40% [4–8].

The same half-cell reaction and characteristics are also important for an effective DMFC cathode, but with a few differences. There is significantly more water at the DMFC cathode due to water crossover from the liquid-fed anode [9,10], in addition to ORR-produced water. On the other hand, a requirement for the DMFC cathode is low air flowrate operation, since water loss from the cell must be controlled and less auxiliary power may be used for portable applications. Under this circumstance, however, removal of product water is inefficient and the cathode catalyst layer must perform well in the presence of slight flooding. The other key difference relates to methanol crossover and the associated cathode voltage loss. In order to mitigate the crossover effect, the cathode catalyst loading has to be increased several times higher than that of a H_2/air cell, corresponding to a much thicker cathode CL. Although the crossover methanol is almost completely oxidized at the DMFC cathode [11], the oxidation reaction not only produces a mixed potential, but also consumes oxygen. Both result in additional oxygen transport limitation through a thick cathode CL, which must be carefully designed in order to optimize the performance.

* Corresponding author. Tel.: +1 814 863 4762; fax: +1 814 863 4848.
E-mail address: cxw31@psu.edu (C.-Y. Wang).

0013-4686/$ – see front matter © 2006 Elsevier Ltd. All rights reserved.
doi:10.1016/j.electacta.2006.08.003

So far, little attention has been paid to *thick* cathode CL structure optimization for portable DMFC application. For high-loading cathodes operated at low air stoichiometry, the existing optimum structure in hydrogen PEM fuel cells must be modified. In this paper, influences of fabrication techniques and ionomer distributions in DMFC cathode CLs are investigated. Various electrochemical methods are combined with surface morphology characterization to closely examine CL structures.

2. Experimental

2.1. Preparation of membrane electrode assembly

Carbon cloth (EC-CC1-060T, ElectroChem Inc.) was used as the cathode backing and carbon-supported Pt catalyst (40% Pt/Vulcan XC72; E-TEK) was used as catalysts. A mixture of Vulcan XC72R carbon black and PTFE emulsion (TFE 30, Dupont) was coated on the carbon cloth to form a microporous layer (MPL). Cathode CLs were made in two configurations: CCM and CDM; while anodes were made in CCM configuration only. The CDM cathodes were prepared by spraying catalyst inks onto the surface of a carbon cloth GDL, and CCM was prepared by the decal method [9]. MEA was obtained by hot-pressing two catalyst-coated PTFE decals (in some cases CDM cathode was used) onto a piece of pretreated Nafion 112 membrane at 125 °C and 100 atm for 3 min.

2.2. TEM micrographs

Cross-sectional TEM specimens of CCM MEAs were prepared by ultramicrotomy. MEAs were first embedded into a suitable resin for 24 h at 60 °C. Low embedding temperatures prevent catalyst grain growth and impose less impact on the microstructure of the catalyst layer. Ultra-thin sections were cut with glass knives in floating water and then transferred to specimen support grids. In this work, TEM observation of cross-sectional specimens was done on a JEOL 2010 operated at 200 kV (LaB_6).

2.3. Electrochemical characterization

A fuel cell fixture with active area of 12 cm^2 was used. The flowfield, consisting of machined two-pass serpentine grooves on graphite blocks, was identical for both anode and cathode. Fuel cell polarization curves were recorded at a quick-scan rate of 20 mA/s. CV measurement was conducted at room temperature with a scan rate of 5 mV/s from 0 to 1.2 V versus DHE, by feeding humidified N_2 and H_2 to the cathode and anode, respectively. The surface roughness of the electrode was evaluated by the amount of charge required to oxidize atomic hydrogen absorbed on Pt electrocatalysts, after correcting the double layer charge (at 0.4 V versus DHE). Assuming a value of 210 $\mu C\,cm^{-2}$ for the oxidation of atomic hydrogen on a smooth Pt surface, surface roughness factor (RF) is obtained by

$$\mathrm{RF} = \frac{S}{v \times 210\,\mu\mathrm{C\,cm^{-2}} \times A} 10^9 \quad (1)$$

where v is the voltage scan rate (5 mV s^{-1}), S the integration area of the hydrogen desorption peak (unit in AV), and A is the electrode geometric area. Electrochemical impedance spectra (EIS) were conducted using a Solartron 1278 electrochemical interface in conjunction with a Solartron 1260 frequency response analyzer, by applying a 10 mV sine wave in the frequency range of 0.1 Hz–10 KHz. Data points were recorded by a software package Zplot.

3. Results and discussion

3.1. Electronic micrographs of cathode catalyst layers

The surface morphologies of a carbon cloth GDL with a pre-coated MPL, a low-loading CDM (0.6 mg Pt cm^{-2}) and a high-loading CDM (1.2 mg Pt cm^{-2}) are shown in Fig. 1a–c, respectively. Scanning electron microscopy (SEM, FEI-Philips XL-20) was used to obtain the images. The cracks on the surface of the MPL provide a path for gas transport to the CL. In Fig. 1b, there are some small cracks and voids scattered on the surface of the catalyst layer. The area between these cracks and voids forms a non-defective layer. Higher catalyst loading and thicker CL would induce higher surface tension, thus causing more severe surface roughness and cracks, commonly referred to as mud cracking, as shown in Fig. 1c.

Fig. 2a and b show the surface morphologies of a low-loading (0.6 mg Pt cm^{-2}) and a high-loading (1.2 mg Pt cm^{-2}) catalyst-coated decal prepared by tape casting, before they are hotpressed onto Nafion membranes. The catalyst and ionomer composite layers form cake-like structures on a Teflon decal. Some uniform and small cracks can be easily identified on the surface of the low-loading decal, while for the high-loading one, although their number declines, the cracks widen and deepen, and the Teflon decal is visible at the bottom of the cracks.

Fig. 3a and b display the TEM images of the CL/membrane interface and bulk of cathode CL in a used CCM MEA, respectively. Recast Nafion in the catalyst layer integrates perfectly with the membrane, and there is an intimate binding between the CL and membrane. The catalyst particles and ionomer are well mixed and uniformly distributed at the microscale. However at the large scale, catalyst particle agglomeration and macro-pores (with diameter about 100 nm) are visible in the bulk of the CL. The agglomeration and macro-pores are defects, which are introduced into the CL during MEA fabrication due to insufficient mixing. The influence of macro-pores on oxygen concentration distribution and cell performance will be theoretically analyzed in Part II of this study.

3.2. Evaluation of different MEAs

In this portion of the work, different MEAs were fabricated with varying catalyst loading, I/C (ionomer to carbon) ratio and ionomer distribution in cathode catalyst layers, as summarized in Table 1. The cathode performance was evaluated in an H_2/air fuel cell instead of a DMFC, since it is difficult to single out the cathode over-potential from a DMFC polarization curve.

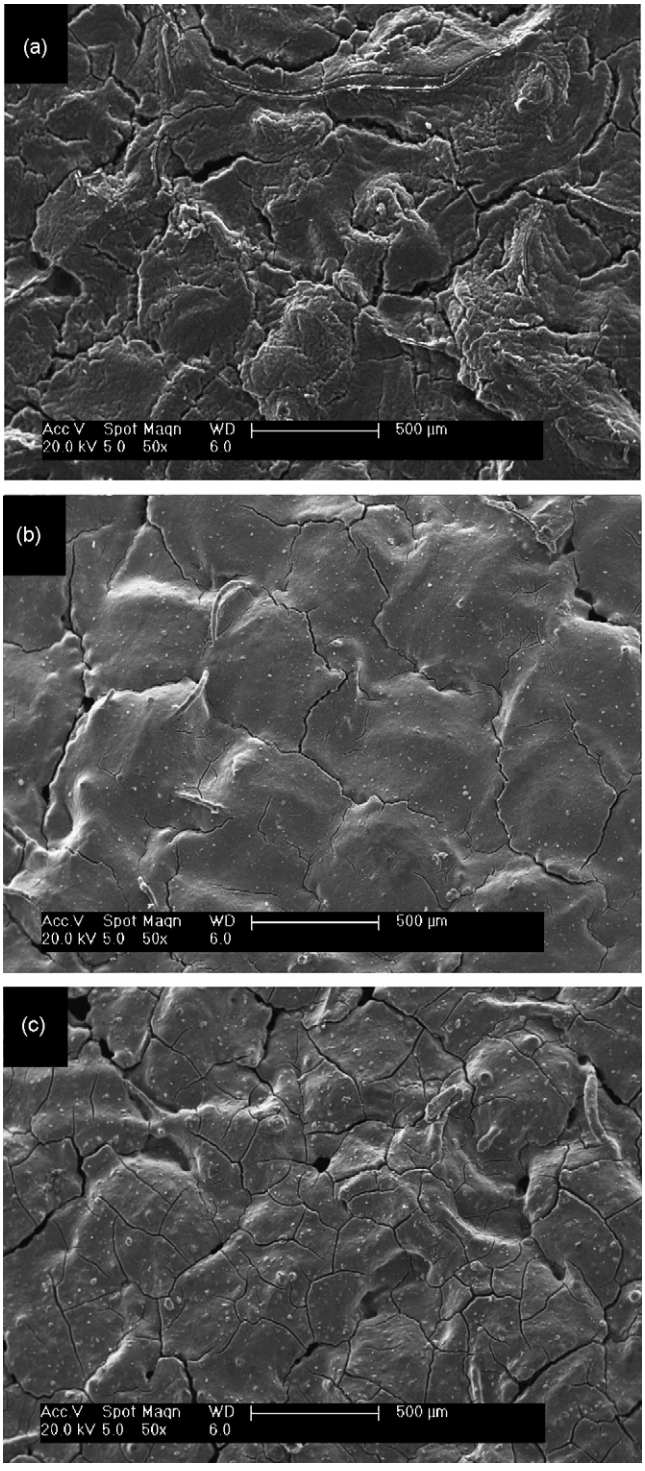

Fig. 1. Surface morphologies of: (a) a carbon cloth GDL; (b) a low-loading CDM (0.6 mg cm^{-2}); (c) a high-loading CDM (1.2 mg cm^{-2}).

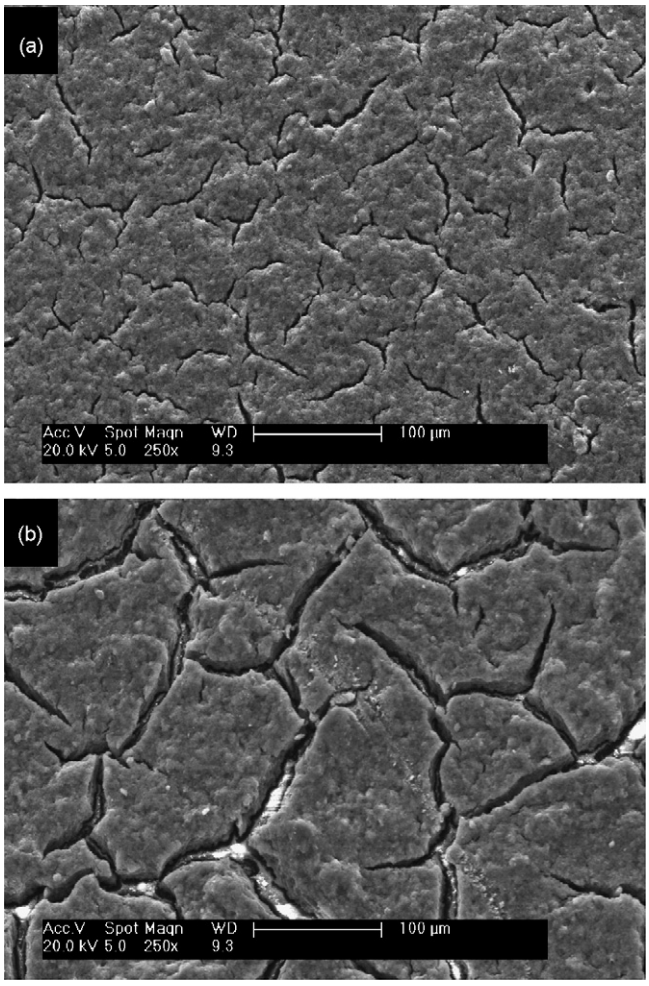

Fig. 2. Surface morphologies of: (a) the low loading (0.6 mg cm^{-2}) and (b) high loading (1.2 mg cm^{-2}) catalyst-coated decals.

3.3. Influence of fabrication techniques

The cell polarization curves for different MEAs are plotted in Fig. 4a and b. The hydrogen flowrate is 100 ml min^{-1}, corresponding to a stoichiometry of ca. 7.3@150 mA cm^{-2}, so the cell performance is only limited by the cathode. Comparing the cell performance of different MEAs at the same Pt loading, i.e., comparing MEA-B and MEA-D, or MEA-A and MEA-C, it is interesting to note that CCM MEAs show better performance than CDM MEAs at low current density regime (40–70 mA cm^{-2}), while the situation is reversed at high current density regime (100–400 mA cm^{-2}). MEA-C has a lower limiting current density, indicating poorer mass transport in the CL. MEA-E, with a composite structure, shows better characteristics than MEA-C and MEA-A at low and high current density regimes, respectively. CDM cathodes have lower open circuit voltage (OCV), only 0.91 and 0.89 V for MEA-C and MEA-D (see Fig. 4a), respectively. This is probably because CDM MEAs do not have intimate CL/membrane interface as CCM MEAs do, since it is difficult for the solid polymer membrane to penetrate into the cracks on the CL surface (Fig. 1). The corresponding Tafel slopes of different MEAs, also indicated in the figure, are obtained by fitting the data points under the current density of 100 mA cm^{-2}. The CDM MEAs (MEA-C and MEA-D) have smaller Tafel slopes than the CCM MEAs (MEA-A and MEA-B), with MEA-E between them.

As a diagnostic tool, the performance of H_2/O_2 cells was also measured. The difference in cell voltage between a pair of H_2/air and H_2/O_2 performance curves is often termed as the

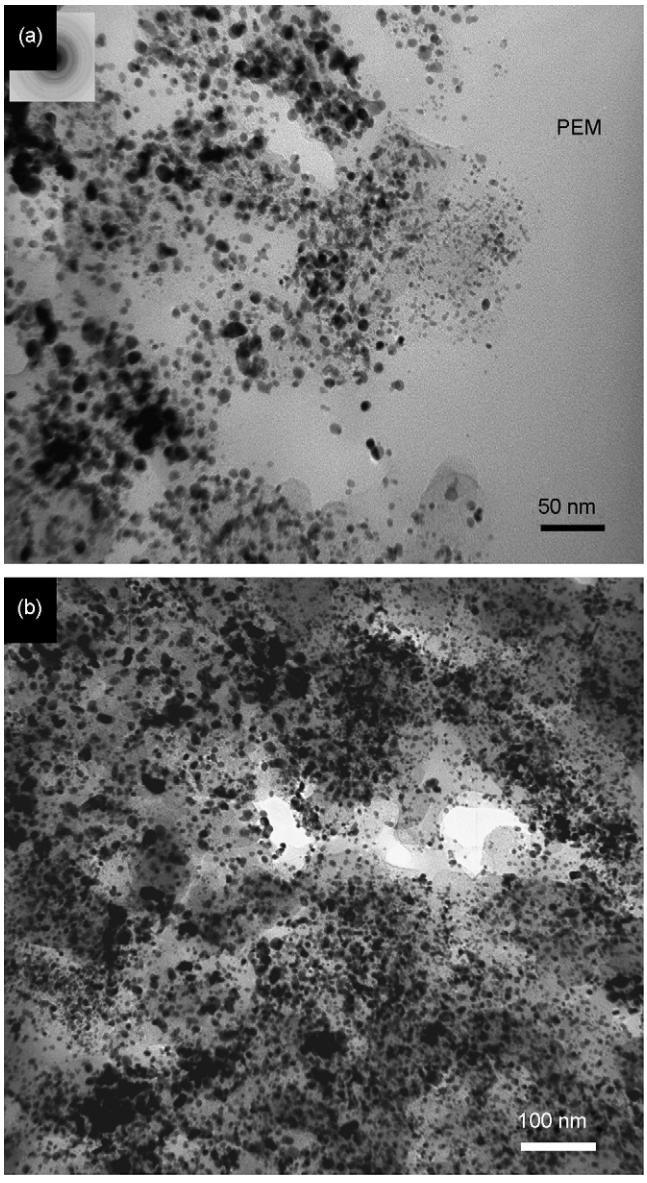

Fig. 3. TEM image of the cathode CL in a used CCM MEA: (a) the interface between the catalyst layer and the polymer membrane and (b) the bulk of the catalyst layer.

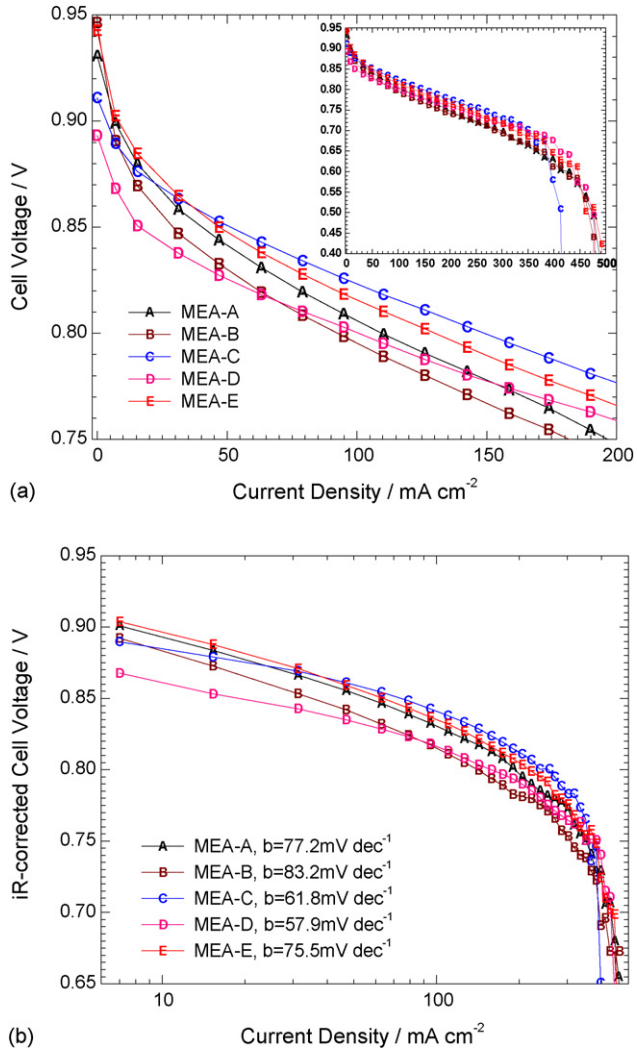

Fig. 4. *iR*-corrected polarization curves of different MEAs. The flowrate of fully humidified H_2 and air was 100 and 97 ml min^{-1} at the anode and cathode, respectively. The air flowrate corresponds to a stoichiometry of 3@150 mA cm^{-2}. The cell was operated at 60 °C and ambient pressure at both anode and cathode.

Table 1
Summary of different MEA specifications

MEA	Anode		Membrane	Cathode	
	Catalyst layer configuration and loadings	I/C ratio		Catalyst layer configuration and loadings	I/C ratio
MEA-A	CCM, 0.6 mg Pt cm^{-2}	1:2.4	NF 112	CCM, 1.2 mg Pt cm^{-2}	1:2.4
MEA-B	CCM, 0.6 mg Pt cm^{-2}	1:2.4	NF 112	CCM, 0.6 mg Pt cm^{-2}	1:2.4
MEA-C	CCM, 0.6 mg Pt cm^{-2}	1:2.4	NF 112	CDM, 1.2 mg Pt cm^{-2}	1:2.4
MEA-D	CCM, 0.6 mg Pt cm^{-2}	1:2.4	NF 112	CDM, 0.6 mg Pt cm^{-2}	1:2.4
MEA-E	CCM, 0.6 mg Pt cm^{-2}	1:2.4	NF 112	Composite structure, MEA-B + MEA-D, 1.2 mg Pt cm^{-2}	1:2.4
MEA-F	CCM, 0.6 mg Pt cm^{-2}	1:2.4	NF 112	CCM, 1.2 mg Pt cm^{-2}	1:2.1
MEA-G	CCM, 0.6 mg Pt cm^{-2}	1:2.4	NF 112	CCM, 1.2 mg Pt cm^{-2}	1:1.8
MEA-H	CCM, 0.6 mg Pt cm^{-2}	1:2.4	NF 112	CCM, 0.6 mg Pt cm^{-2}	1:1.8
MEA-I	CCM, 0.6 mg Pt cm^{-2}	1:2.4	NF 112	Composite structure, MEA-H + MEA-D, 1.2 mg Pt cm^{-2}	–

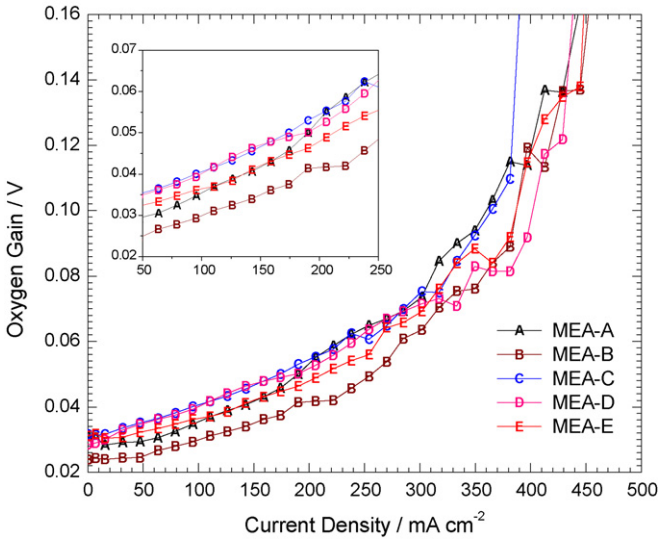

Fig. 5. Oxygen gains of different MEAs at 60 °C.

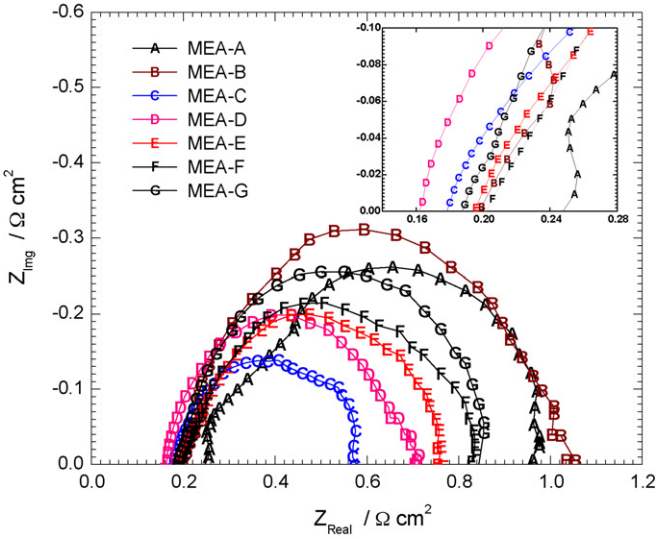

Fig. 6. EIS results of different MEAs using air (at 0.8 V). The operating conditions were the same as in Fig. 4.

oxygen gain [12] and can be expressed as

$$\Delta E_{O_2/air} = E_{O_2} - E_{air} \quad (2)$$

Fig. 5 displays the oxygen gains of different MEAs at 60 °C and cathode stoichiometry $\xi_c = 3@150\,mA\,cm^{-2}$. Higher oxygen gain is a qualitative indicator of mass-transport loss in a CL structure that, for instance, floods easily. Between 50 and 250 mA cm^{-2}, CDM cathodes show higher oxygen gain, and thus more severe mass-transport resistance than CCM cathodes. The high-loading CCM MEA (MEA-A) also shows high mass-transport resistance at higher current densities.

The different behaviors of CCM and CDM MEAs are probably caused by their different Pt distributions in the CLs. After the catalyst-coated decals (Fig. 2) are hotpressed to the membranes to form CCMs, catalysts are distributed uniformly between the membrane and GDL. In CDM, part of the catalysts sprayed on the GDL surface may settle internally, thus the catalysts are located preferentially near the GDL. When a current is applied, especially at low air stoichiometry, the oxygen concentration profile in the CL may not be uniform, starting to decline from the catalyst layer/GDL interface and reaching the lowest value toward the CL/membrane interface. In the presence of an oxygen concentration gradient, all the catalytical sites are not equally accessed by the oxygen; that is, the catalysts near the membrane contribute less to the overall electrochemical reaction than those near the GDL. Thus, CDM MEAs, with more catalyst near the GDL/CL interface, probably have higher catalyst utilization and higher performance at moderate current density.

Fig. 6 displays the EIS results of different MEAs at 0.8 V cell voltage for H_2/air fuel cells. The high-frequency portion is shown in the inset. As expected, semi-circular loops that correspond to ORR are observed. Higher Pt loading reduces the ORR resistance, as indicated by smaller semi-circles. At high frequencies, a Warburg-like response (45° slope) is observed, especially for high-loading CCM (MEA-A), which corresponds to the ion migration and capacitance between agglomerates within the catalyst layer. The intercept of EIS spectra with the real axis at high frequency corresponds to the internal ohmic resistance of the cell, R_Ω, which represents the sum of uncompensated resistance in the CL, membrane, backings, graphite end plates and the contact resistance between them. Another important parameter that can be derived from the EIS results is R_p, which corresponds to the charge-transfer resistance of ORR [13]. The values of R_Ω and R_p of different MEAs are listed in Table 2. Low-loading MEAs have a thinner catalyst layer, and thus low R_Ω. However, their R_p values are higher than high-loading MEAs. At the same catalyst loading, CCM has slightly larger R_Ω than that of CDM. High-loading CDM (MEA-C) shows the smallest R_p value, 0.524 and 0.578 Ω cm^2 under oxygen and air, respectively; while low-loading CCM (MEA-B) has the largest R_p values. The ratios of R_p values between oxygen and air operation are also listed in Table 2. For the same MEA under air and oxygen operation, the

Table 2
Data obtained from EIS results

MEA	Oxygen operation		Air operation		Ratio of R_p under oxygen and air
	R_Ω (Ω cm^2)	R_p (Ω cm^2)	R_Ω (Ω cm^2)	R_p (Ω cm^2)	
MEA-A	0.280	0.867	0.248	0.955	0.830
MEA-B	0.196	1.025	0.198	1.033	0.993
MEA-C	0.183	0.524	0.178	0.578	0.853
MEA-D	0.167	0.639	0.162	0.703	0.873
MEA-E	0.207	0.715	0.195	0.755	0.906

only differences are oxygen concentration and diffusion. Therefore, the ratio has the same characteristics as the oxygen gain. A larger ratio (approaching unity) represents more favorable oxygen transport through the CL. MEA-B (low-loading CCM) has the biggest R_p ratio, and MEA-C (high-loading CDM) has the smallest R_p ratio. It seems that CCM is a good choice for low-Pt-loading MEA, but high-loading CCM may result in large cell internal resistance and mass transport limitation.

The above experimental observation is consistent with the CL thickness measurement, conducted by a Mitutoyo electronic dial indicator. Measurements were performed for at least five different locations and the averaged thickness of MEA-A, B, C and D are 23.2, 12.7, 22.6 and 10.4 μm, respectively. The porosities can thus be evaluated by the following equation

$$\varepsilon_{CL} = 1 - \left[\frac{1}{\rho_{Pt}} + \frac{1.5}{\rho_c} + \frac{1.5 \times SW \times R_{I/C}}{\rho_{Nafion}}\right] \frac{L_{Pt}}{\Delta X_{CL}} \quad (3)$$

where ε_{CL} is the porosity, $R_{I/C}$ is the I/C ratio, SW is the swelling degree of dry ionomer upon hydration by weight (120%), and L_{Pt} is the Pt loading. In the above equation, 1.5 corresponds to the weight ratio of carbon to Pt in 40% Pt/C catalyst. The porosities are estimated to be 0.38, 0.44, 0.37 and 0.31, for MEA-A, B, C and D, respectively. Small porosities in cathode CLs of MEA-C and D may cause severe oxygen transport resistance when operated at small air stoichiometry.

3.4. Influence of ionomer content and distribution

Fig. 7 compares the *iR*-corrected polarization curves of H_2 PEM fuel cells of MEA-A, MEA-F and MEA-G at 60 °C using different oxidants. I/C ratios of these MEAs are 1:2.4, 1:2.1 and 1:1.8, respectively; that is, MEA-G has the largest ionomer content, while MEA-A has the smallest. MEA-F and MEA-G have higher OCV than MEA-A in both air and oxygen. The three MEAs produce almost identical performance in oxygen. When air was used as the oxidant, different MEAs have almost identical performance at lower current density region (<100 mA/cm^2), with MEA-F and MEA-G showing slightly higher cell voltages. At higher current densities, their behaviors differ markedly. The cell voltage of MEA-G bends downwards dramatically with current density and the limiting current density is smaller than 400 mA/cm^2. MEA-A, which has the smallest Nafion content, can extend current density to higher values, ca. 500 mA/cm^2, while the limiting current density of MEA-F is slightly lower, although it shows the best performance in the moderate current density. Porosity in the CL is inversely proportional to its ionomer content. MEA-G has the smallest porosity, thus the worst mass transport. MEA-A has the largest porosity; however, at the same time, the effective proton conductivity of the CL is sacrificed. This analysis agrees well with the EIS results as shown in Fig. 6. MEA-G has the smallest R_Ω, while MEA-A has the largest R_Ω and R_p. MEA-F has the smallest R_p, which is consistent with its superior performance. MEA-F seems to have the best compromise between the oxygen mass transport and proton conduction. Nafion weight fraction is only 22% in the cathode CL of MEA-F, much smaller than that in H_2/air cells.

In the CV results shown in Fig. 8, the charge required for hydrogen desorption (below 0.4 V) is used to evaluate the roughness factor of the electrodes according to Eq. (1), namely 290, 381, and 349 cm^2 cm^{-2} for MEA-A, MEA-F and MEA-G, respectively. When increasing the ionomer content in the catalyst layer, the roughness factor or electrochemically active area (ECA) seems to increase at first, but it then starts to decrease when the ionomer content is beyond a certain point. When fabricating CL by mixing the catalyst with ionomer solution, some Pt active area is not available for the electrochemical reaction due to either insufficient contact with the electrolyte, or electrical isolation of catalyst particles from each other by the non-conducting Nafion film. MEA-F seems to possess a good balance.

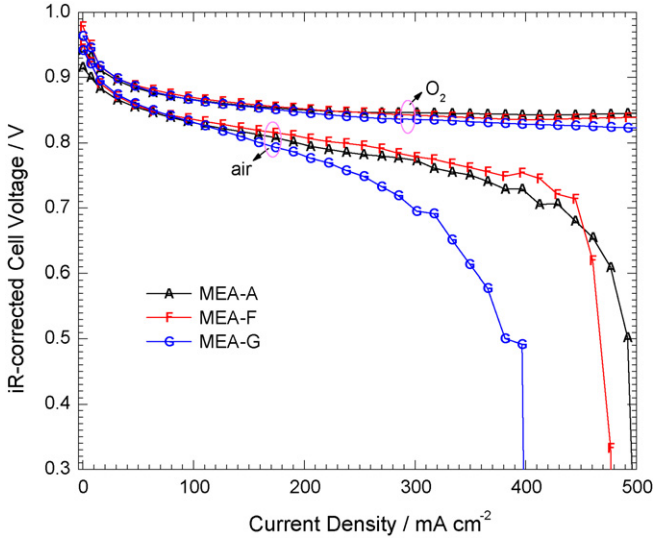

Fig. 7. *iR*-corrected polarization curves of different MEAs using air and oxygen. The flowrate of fully humidified H_2 and oxygen was 100 and 97 ml min^{-1} at the anode and cathode, respectively. The air flowrate is 97 ml min^{-1}. The cell was operated at 60 °C and ambient pressure at both anode and cathode.

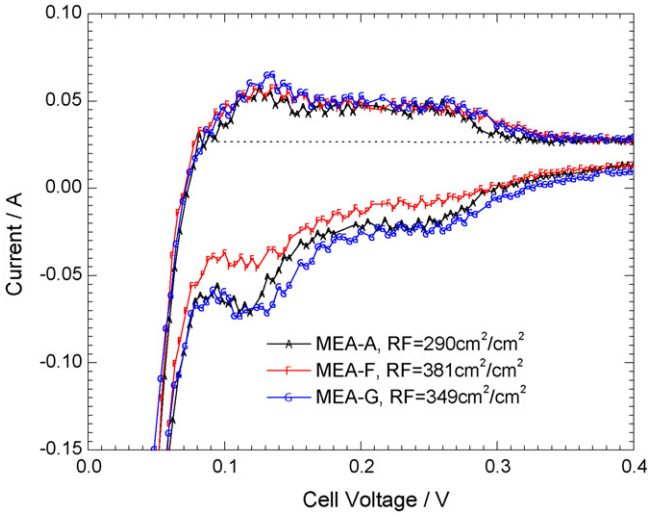

Fig. 8. Cyclic voltammetry (CV) curves of different MEAs. The results were obtained at room temperature and fully humidified H2 and N_2 were fed into the anode and cathode, respectively. The surface roughness factors are also shown.

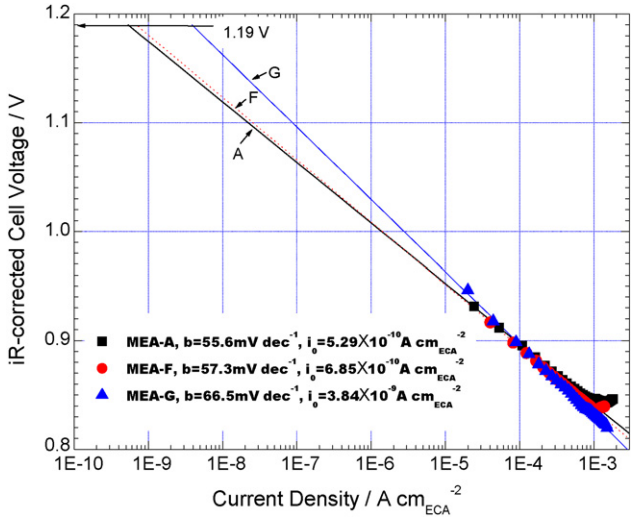

Fig. 9. Hydrogen/oxygen performance curves corrected for ohmic losses at 60 °C. The current densities are normalized to the surface roughness of different MEAs.

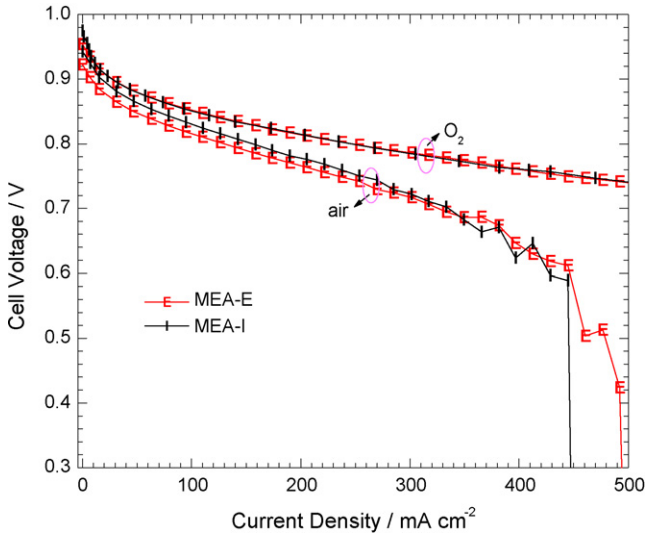

Fig. 10. Polarization curves of different MEAs using air and oxygen. The operating conditions were the same as in Fig. 7.

Fig. 9 shows the *iR*-corrected H_2/O_2 cell performance curves with the current density normalized to the surface roughness. The thermodynamic open circuit potential (E_{rev}) at 60 °C and ambient pressure is estimated to be ~1.19 V using the following equation [14]:

$$E_{rev} = 1.23 - 0.9 \times 10^{-3}(T - 298) + \frac{RT}{4F} \ln(p_{H_2}^2 p_{O_2}) \quad (4)$$

The exchange current densities, obtained by extending the fitted Tafel slopes to 1.19 V, are 5.29×10^{-10}, 6.85×10^{-10} and 3.84×10^{-9} A cm_{ECA}^{-2} for MEA-A, MEA-F and MEA-G, respectively. It seems that higher Nafion loading in the CL increases the exchange current density, probably due to the increased oxygen solubility and hence higher concentration at the ionomer/catalyst interface [15,16].

The effect of ionomer distribution in the CL on cell performance is demonstrated in Fig. 10. Both MEAs have composite cathode structures but different ionomer distributions: MEA-E has identical I/C ratio throughout its catalyst layer; while MEA-I has non-uniform ionomer distribution, with higher I/C ratio near the membrane and lower I/C ratio near the GDL. The two composite MEAs were made by hotpressing a CDM to a CCM at 125 °C and 100 atm for 1 min. The two MEAs have almost identical performance using oxygen. However, MEA-I shows better features using air, i.e., higher OCV and higher cell voltage in moderate current density regime, although its limiting current density is slightly lower than that of MEA-E.

Appropriate pore size and distribution in the CL are very important to reduce the mass transport resistance and realize uniformly high catalyst utilization. Large porosity facing the GDL in the CL facilitates gas access to the catalytic sites, increasing the limiting current density; small porosity (or higher density of Nafion and Pt composite) near the membrane/CL interface increases the oxygen solubility and hence the ORR kinetics. MEA-E and MEA-I show better characteristics than MEA-A and MEA-C because they have better pore distribution in the cathode CLs, so that the porosity variation across the CL favors both oxygen solubility and oxygen transport, resulting in better ORR kinetics and higher limiting current density.

3.5. Cathode performance evaluation in DMFCs

As discussed earlier, the polarization curves of the MEA with composite CL structures show better features in both kinetic and mass-transport regimes than those with pure CDM and CCM structures. Therefore, the subsequent research work was to evaluate its performance in DMFCs.

One MEA using the same cathode as MEA-E was fabricated. The anode is in the configuration of CCM with a PtRu loading of about 4.5 mg/cm^2. Fig. 11 shows the quick-scan performance of

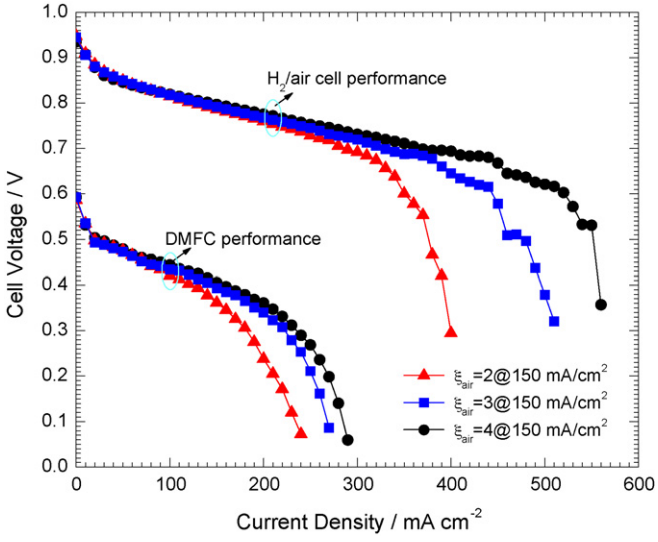

Fig. 11. Polarization curves of an H_2/air fuel cell and DMFC at different air stoichiometries. 2 M methanol solution was used in DMFC operation and its flowrate corresponds to a stoichiometry of 2@150 mA/cm^2. Other operating conditions were the same as in Fig. 7.

a DMFC and an H_2/air cell. All the polarization curves clearly show the kinetic, ohmic and mass-transport regimes. The DMFC performance shows much smaller limiting current densities than the H_2/air cell, due to additional mass-transport limitation at the anode. The H_2/air cell yields voltages of 0.797 and 0.786 V at air stoichiometries of 4 and 2@150 mA/cm^2, respectively, while the DMFC produces much lower cell voltages of only 0.406 and 0.362 V at the same air stoichiometries, which corresponds to power densities of 60.1 and 54.3 mW/cm^2, respectively. It seems that DMFC performance is more sensitive to air stoichiometry, and there is a minimum air flowrate required to sustain efficient and stable operation. It is believed that the crossover methanol from the anode is almost completely converted to carbon dioxide and water in the presence of the cathode catalyst; however, this reaction consumes oxygen from the air supplied to the cathode that would otherwise be required for the oxygen reduction reaction [17]. It is estimated that at a methanol crossover current of 100 mA/cm^2, the air needed for methanol oxidation is roughly 20 SCCM, which is almost 1/3 of the air flowrate at stoichiometry of 2@150 mA/cm^2.

To evaluate the cathode performance in a DMFC, if the over-potentials of hydrogen-evolving and hydrogen-oxidizing electrodes are negligibly small, the following equation can be used [18]:

$$E_{\text{Air}}^{\text{MeOH}}(I) = E^{*}_{\text{MeOH/Air}}(I) + E^{*}_{\text{MeOH/H}_2}(I) \quad (4)$$

where the asterisk designates '*iR*-free', $E_{\text{Air}}^{\text{MeOH}}(I)$ is the air cathode potential at relevant DMFC conditions that contains the effects of methanol crossover and mixed over-potential, and where $E^{*}_{\text{MeOH/Air}}(I)$and $E^{*}_{\text{MeOH/H}_2}(I)$ are the *iR*-free voltages under DMFC and anode polarization modes. From the EIS results (not shown here), the cell ohmic resistances are nearly identical under the DMFC and anode polarization modes, ca. 0.181 Ω cm^2, so Eq. (4) can be simplified as

$$E_{\text{Air}}^{\text{MeOH}}(I) = E_{\text{MeOH/Air}}(I) + E_{\text{MeOH/H}_2}(I) \quad (5)$$

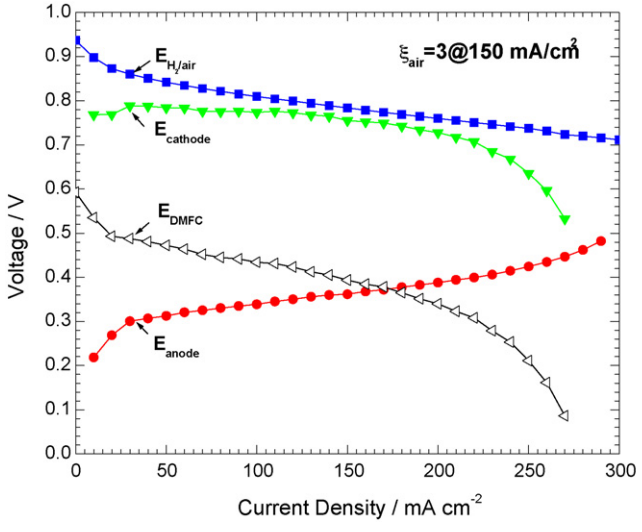

Fig. 12. Quick-scan polarization curves under different operating modes, including DMFC, anode polarization, and the evaluated cathode performance. Refer to Fig. 11 for operating details.

Fig. 12 shows the quick-scan polarization curves under different operating modes, including H_2/air, DMFC, anode polarization, and the evaluated cathode performance using Eq. (5). The DMFC and anode polarization curves have almost identical limiting current densities, indicating that the maximum DMFC current is limited by the anode. The evaluated cathode performance approaches that of the H_2/air cell at high current densities, where methanol crossover and hence its detrimental effects become trivial. At 150 mA/cm^2 a potential reduction of ~27 mV due to methanol crossover is observed, which is slightly larger than the value (20 mV for NF117) reported by Thomas et al. [18] at the same operating temperature. Since they used only 0.5 M methanol solution and a much thicker membrane (NF117), it is reasonable to expect a smaller methanol crossover.

4. Conclusion

Fabrication techniques have a large influence on the performance of cathode CLs of DMFCs. CCM and CDM MEAs have different Pt catalyst distributions in their CLs, and CCM MEAs have higher cell OCVs and produce higher cell voltages at lower current densities (<50 mA cm^{-2}). However, at higher current densities, their performances are inferior to those of CDM MEAs. More catalysts are supposed to locate near the GDL in the CDM CL, resulting higher Pt utilization at higher current density. Composite structures, consisting of both CCM and CDM, have better porosity distribution, thus better polarization characteristics. In the CLs with appropriate ionomer distributions, the porosity variation across the catalyst layers favors both oxygen solubility, oxygen transport and proton conduction, resulting in better ORR kinetics and higher limiting current density. DMFC performance is more sensitive to the air stoichiometry, and there is a minimum air flowrate required to sustain efficient and stable operation of the cathode. The evaluated cathode performance in the DMFC approaches that of the H_2/air cell at high current densities, where methanol crossover and hence its detrimental effects become trivial. At 150 mA/cm^2, a potential reduction of ~27 mV due to methanol crossover is observed.

References

[1] S.J. Lee, S. Mukerjee, J. McBreen, Y.W. Rho, Y.T. Kho, T.H. Lee, Electrochim. Acta 43 (1998) 3693.
[2] M. Uchida, Y. Aoyama, N. Eda, A. Ohta, J. Electrochem. Soc. 142 (1995) 463.
[3] M. Uchida, Y. Fukuoka, Y. Sugawara, H. Ohara, A. Ohta, J. Electrochem. Soc. 145 (1998) 3708.
[4] E. Antolini, L. Giorgi, A. Pozio, E. Passalacqua, J. Power Sources 77 (1999) 136.
[5] E. Passalacqua, F. Lufrano, G. Squadrito, A. Patti, L. Giorgi, Electrochim. Acta 46 (2001) 799.
[6] J.M. Song, S.Y. Cha, W.M. Lee, J. Power Sources 94 (2001) 78.
[7] Z. Qi, A. Kaufman, J. Power Sources 113 (2003) 37.
[8] G. Sasikumar, J.W. Ihm, H. Ryu, J. Power Sources 132 (2004) 11.
[9] G.Q. Lu, F.Q. Liu, C.Y. Wang, Electrochem. Solid-State Lett. 8 (2005) A1.
[10] F.Q. Liu, G.Q. Lu, C.-Y. Wang, J. Electrochem. Soc. 153 (2006) A543.
[11] X.M. Ren, S. Gottesfeld, J. Electrochem. Soc. 148 (2001) A87.

[12] S. Kocha, in: W. Vielstich, A. Lamm, H.A. Gasteiger (Eds.), Handbook of Fuel Cells—Fundamentals, Technology and Applications, vol. 3, Wiley, Chichester, 2003, p. 538.
[13] C.H. Hsu, C.C. Wan, J. Power Sources 115 (2003) 268.
[14] D.M. Bernardi, M.W. Verbrugge, J. Electrochem. Soc. 139 (1992) 2477.
[15] S. Gottesfeld, T. Zawodzinski, in: R. Alkire, H. Gerischer, D. Kolb, C. Tobias (Eds.), Advances in Electrochemical Science and Engineering, vol. 5, Wiley-VCH, Weinheim, 1988, p. 246.
[16] J. Xie, F. Garzon, T. Zawodzinski, W. Smith, J. Electrochem. Soc. 151 (2004) A1084.
[17] J. Müller, G. Frank, K. Colbow, D. Wilkinson, in: W. Vielstich, A. Lamm, H.A. Gasteiger (Eds.), Handbook of Fuel Cells—Fundamentals, Technology and Applications, vol. 3, Wiley, Chichester, 2003 (Chapter 62).
[18] S.C. Thomas, X. Ren, S. Gottesfeld, P. Zelenay, Electrochim. Acta 47 (2002) 3741.